LETTERS

Seasonal characteristics of the Indian Ocean Dipole during the Holocene epoch

Nerilie J. Abram[1]†, Michael K. Gagan[1], Zhengyu Liu[2,3,4], Wahyoe S. Hantoro[5], Malcolm T. McCulloch[1] & Bambang W. Suwargadi[5]

The Indian Ocean Dipole[1,2] (IOD)—an oscillatory mode of coupled ocean–atmosphere variability—causes climatic extremes and socio-economic hardship throughout the tropical Indian Ocean region[1–5]. There is much debate about how the IOD interacts with the El Niño/Southern Oscillation (ENSO) and the Asian monsoon, and recent changes in the historic ENSO–monsoon relationship[6] raise the possibility that the properties of the IOD may also be evolving. Improving our understanding of IOD events and their climatic impacts thus requires the development of records defining IOD activity in different climatic settings, including prehistoric times when ENSO and the Asian monsoon behaved differently from the present day. Here we use coral geochemical records from the equatorial eastern Indian Ocean to reconstruct surface-ocean cooling and drought during individual IOD events over the past ~6,500 years. We find that IOD events during the middle Holocene were characterized by a longer duration of strong surface ocean cooling, together with droughts that peaked later than those expected by El Niño forcing alone. Climate model simulations suggest that this enhanced cooling and drying was the result of strong cross-equatorial winds driven by the strengthened Asian monsoon of the middle Holocene. These IOD–monsoon connections imply that the socioeconomic impacts of projected future changes in Asian monsoon strength may extend throughout Australasia.

The IOD, also termed the Indian Ocean Zonal Mode, involves a reversal of the sea surface temperature (SST) gradient and winds across the equatorial Indian Ocean from their climatological state. Climate simulations suggest that IOD events can be initiated by El Niño conditions that decrease the thermocline depth in the Indonesian throughflow region, and cause an eastward migration of the Pacific Walker circulation cell (which encourages atmospheric subsidence over the eastern Indian Ocean)[7,8]. Simulations also indicate that IOD events can result from processes internal to the Indian Ocean region, through intensified Hadley circulation of the Asian–Australian monsoon, which strengthens the southeasterly tradewinds and promotes upwelling of cooler water in the equatorial eastern Indian Ocean[7,8]. However, the ability to test these simulations is restricted by the spatial limitations and brevity of high-quality historical climate records (Supplementary Fig. 1) and the scarcity of proxy records[4,9], particularly in the eastern IOD region.

High-resolution reconstructions of past climate in the tropical ocean regions can be obtained through the analysis of geochemical tracers in the skeletons of massive *Porites* sp. corals. The coral reefs of the Mentawai Islands, western Indonesia, lie within the eastern Indian Ocean sector used to define the Dipole Mode Index of IOD activity[2] (Fig. 1a). During strong IOD events, upwelling in the eastern IOD sector results in anomalous cooling of SSTs and intense drought. An unambiguous record of these eastern IOD SST and rainfall anomalies can potentially be provided through coupled measurements of Sr/Ca (a proxy for SST[10]) and oxygen isotope ratios ($\delta^{18}O$; a proxy for SST and changes in rainfall/evaporation[11]) in corals from the Mentawai Islands. Furthermore, great palaeoearthquakes along the Mentawai island arc[12] have frequently uplifted the fringing reefs surrounding the Mentawai Islands, leaving individual fossil *Porites* colonies well-preserved in growth position. This

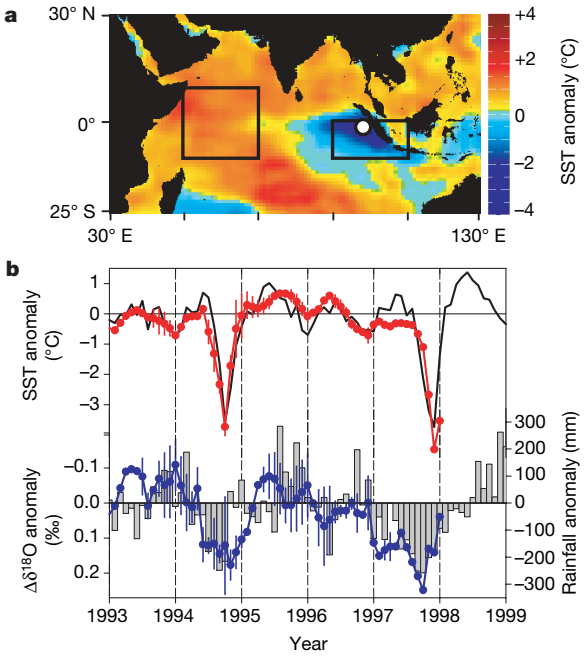

Figure 1 | IOD climate anomalies. a, SST anomalies during November of the 1997 IOD event[13], when anomalous cooling in the east and warming in the west produced a reversal of the equatorial SST gradient across the Indian Ocean. Boxes mark the eastern and western sectors used to define the Dipole Mode Index[2], and the white circle shows the location of the Mentawai Islands. **b**, In the Mentawai Islands the strong IOD events of 1994 and 1997 were characterized by cool SST anomalies (black curve)[13] and drought (grey bars)[29]. These distinct IOD SST and rainfall anomalies are preserved, respectively, in coral Sr/Ca–SST (red curve) and $\Delta\delta^{18}O$ (blue curve) anomalies[11]. Coral time series between July 1993 and February 1997 are based on the average of two coral records, with error bars showing the difference between the coral records for each monthly data point.

[1]Research School of Earth Sciences, The Australian National University, Canberra, Australian Capital Territory 0200, Australia. [2]Center for Climatic Research, University of Wisconsin-Madison, 1225 W. Dayton Street, Madison, Wisconsin 53706, USA. [3]Earth Environment Institute, Chinese Academy of Science, Xi'an 710075, China. [4]The Ocean University of China, Qingdao 266003, China. [5]Research and Development Center for Geotechnology, Indonesian Institute of Sciences (LIPI), Bandung 40135, Indonesia. †Present address: British Antarctic Survey, Natural Environment Research Council, Cambridge CB3 0ET, UK.

allows us to examine the ocean–atmosphere signatures of individual IOD events for slices of time since ~6,500 calibrated years before present (BP).

To test the suitability of Mentawai corals for reconstructing IOD SST and rainfall anomalies, Sr/Ca and $\delta^{18}O$ were analysed at high (~monthly) resolution in two modern corals from the Mentawai Islands (Supplementary Methods). Both corals were collected in open, fore-reef slope environments on fringing reef systems, at water depths of 1.2 m (coral TN99-A-4) and ~6 m (coral TM01-A-10; Supplementary Table 1). Both provide a record of the strong IOD event in 1994. The TM01-A-10 coral record also extends into the 1997 IOD event, when the Mentawai reefs experienced widespread coral mortality[4]. The coral Sr/Ca–SST anomalies reliably reconstruct both the timing and magnitude of IOD cooling during 1994 and 1997, as documented by blended buoy, ship and satellite SST records[13] (Fig. 1b, Supplementary Figs 1 and 2). The coral records of residual $\delta^{18}O$ ($\Delta\delta^{18}O$), determined by using the Sr/Ca–SST records to remove the temperature component of coral $\delta^{18}O$ measured for the same samples, reflect changes in the $\delta^{18}O$ composition of sea water that are due to variations in the surface–ocean balance of rainfall and evaporation[11]. Comparison with station and gridded rainfall data shows that the Mentawai coral $\Delta\delta^{18}O$ records replicate the droughts in western Indonesia that accompanied the 1994 and 1997 IOD events (Fig. 1b).

The distinct cool/dry IOD signal in the Mentawai coral Sr/Ca and $\delta^{18}O$ records indicates that corals from the eastern upwelling region can be used as an independent proxy for strong IOD activity. Further analysis of a 140-year-long coral record from the Mentawai Islands has identified two more exceptionally strong IOD signals in 1961 and 1877 AD[4] (Supplementary Fig. 3). Both years were times of extreme climate in the Indian Ocean region[2,5,14,15], consistent with strong IOD events. Indeed, 1961, 1994 and 1997 correspond with the three strongest droughts in the rainfall record of the Padang-Tabing station in western Indonesia (1° S, 100° E), which was established as part of an extensive network of Indonesian rainfall stations following the devastating drought of 1877 (ref. 15). The modern coral records suggest that strong IOD events occur in both El Niño (1877, 1994 and 1997) and non-El Niño (1961) years, consistent with climate simulation results[7,8]. IOD events also appear to exist over a wide range of monsoon conditions, with the 1877 IOD event corresponding to a year of extreme monsoon failure, while the 1961 IOD occurred during the heaviest monsoon in the nearly 200-year-long all-India monsoon rainfall index[16]. Hence, understanding how the IOD, ENSO and Asian monsoon systems interact has important implications for the predictability of climate extremes in the Indian Ocean region.

During the early to middle Holocene, broad-scale strengthening of the Asian summer monsoon occurred owing to increased Northern Hemisphere summer insolation[17]. At the same time, ENSO variability was suppressed[18,19] and a more La Niña-like mean state existed across the tropical Pacific Ocean[20]. Thus, mid-Holocene fossil corals from the Mentawai Islands provide a good opportunity to examine how externally forced increases in Asian monsoon strength (which have been predicted for the coming century[21–23]) may influence the IOD system. To do this, reconstructions of four individual IOD events from the middle Holocene (6,570–4,160 calibrated years BP; Fig. 2) were averaged to produce a composite IOD event for a period of strong Asian monsoon forcing (Fig. 3, Supplementary Fig. 3, Supplementary Table 2). For comparison, a composite IOD event was also constructed using four late Holocene IOD events (from 2,180 calibrated years BP to the present), when the Asian monsoon weakened and El Niño events were relatively strong and frequent.

Comparison of the composite SST anomalies shows that, on average, the magnitude of cooling during strong eastern IOD upwelling events is similar for the strong El Niño and strong monsoon scenarios (Fig. 3; -3.9 ± 0.2 °C and -4.3 ± 0.6 °C, respectively). The timing of peak IOD cooling also appears to have remained essentially constant with respect to the seasonal cycle of SST. Today, the timing of peak IOD cooling is constrained by the cross-equatorial wind reversal at the end of the Asian summer monsoon season (November), which brings an abrupt end to Ekman upwelling and cooling along the coast of Sumatra[1]. Thus, the similarity of the seasonal timing of IOD

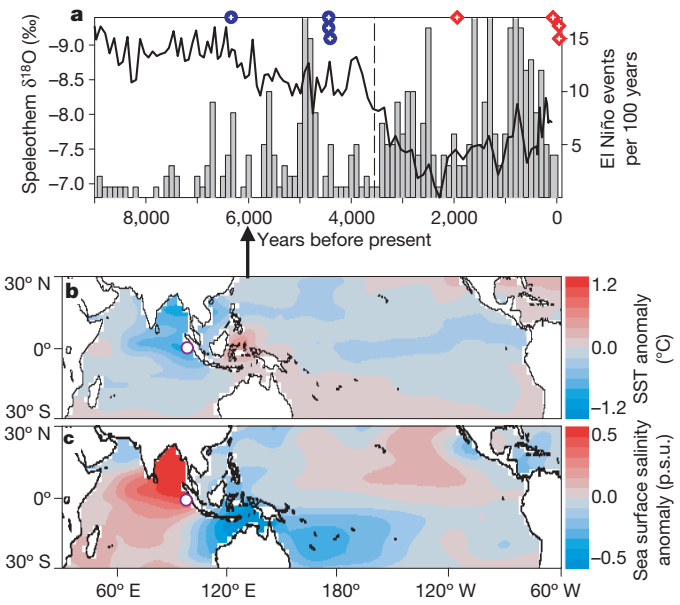

Figure 2 | Monsoon–ENSO–IOD evolution during the Holocene. **a**, Holocene evolution of the Asian summer monsoon and El Niño, as recorded by a speleothem $\delta^{18}O$ record from Dongge Cave, China[17] (black curve) and lake sediments from Laguna Pallcacocha, Ecuador[18] (grey bars), respectively. The dashed vertical line approximately marks the shift from strong monsoon activity during the early–middle Holocene to strong El Niño activity in the late Holocene. Approximate ages of IOD events reconstructed using Mentawai corals (Fig. 3 and Supplementary Fig. 3) are shown by blue circles (strong monsoon scenario) and red diamonds (strong El Niño scenario). In the eastern Indian Ocean, climate simulations (FOAM[24,25]) for 6,000 calibrated years BP produce cooler mean annual SSTs (relative to the present day) that result in a more IOD-like mean state (**b**) and a widespread increase in mean annual sea surface salinity (p.s.u., practical salinity units) (**c**). The white circles in **b** and **c** show location of the Mentawai Islands.

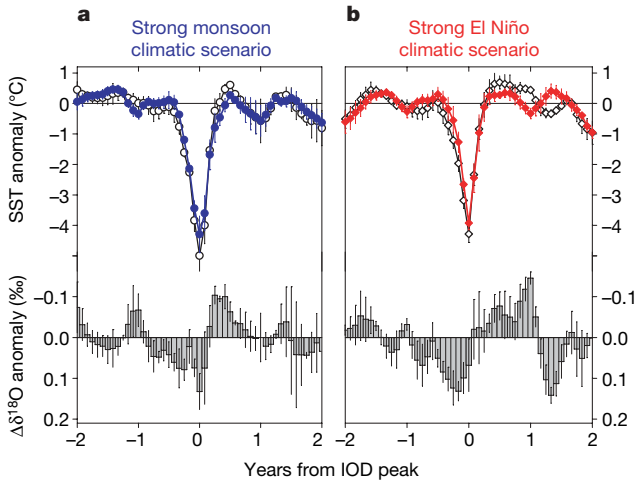

Figure 3 | Composite records of eastern IOD upwelling events. Composite coral Sr/Ca–SST (coloured curves), $\delta^{18}O$ (black curves; shown on an apparent-SST scale) and $\Delta\delta^{18}O$ (grey bars) anomalies were produced for IOD events during periods of strong monsoon activity (middle Holocene) (**a**) and strong El Niño activity (late Holocene) (**b**). Each IOD composite was produced using coral records of four individual eastern IOD upwelling events (Supplementary Fig. 3 and Supplementary Table 2). Error bars show the standard error for each monthly value of the composite IOD profiles.

upwelling events within both climatic scenarios implies that the monsoon wind reversal has been a consistent factor controlling the timing of peak eastern IOD cooling.

Although the magnitude and seasonal timing of peak cooling in the eastern IOD sector is similar for both climatic scenarios, the duration of the cool SST anomaly is greater during times of strong monsoon forcing. Cool anomalies exceeding 1.6 °C (that is, twice as much cooling as the average annual minimum of modern SST in the Mentawai Islands[13]) span five months under the strong monsoon forcing of the middle Holocene (Fig. 4). During the late Holocene, however, the same magnitude of IOD cooling is constrained to three months. It is unlikely that this result is an artefact related to differences in intra-annual coral growth because there is no systematic difference between the average annual cycles of Sr/Ca–SST and $\Delta\delta^{18}O$ recorded by the middle and late Holocene corals (Supplementary Fig. 4).

To examine the physical processes that may have led to extended IOD cooling during the strong monsoon scenario of the middle Holocene, we used orbitally forced simulations of Indian Ocean climate from two coupled ocean–atmosphere models, the Fast Ocean Atmosphere Model (FOAM) and NCAR-CCSM1[24,25]. Under the orbital conditions of 6,000 calibrated years BP, FOAM documents an increase in mean monsoon strength and a mean La Niña-like state in the tropical Pacific that is in good agreement with palaeoclimate reconstructions[24,25]. At the same time, the simulated mean annual SST in the Indian Ocean shows the clear signature of a positive IOD state due to cooling of the surface ocean in the eastern IOD upwelling region (Fig. 2b). This IOD-like mean state is a robust result that is obtained in experiments with both models throughout the early to middle Holocene. The simulated mean SST cooling in the eastern IOD region during the early to middle Holocene is the result of strengthened Asian monsoon winds in both the summer and winter driven by the enhanced seasonal cycle of insolation. The enhanced Asian summer monsoon produces anomalously strong southeasterly winds in the Mentawai region, while the enhanced winter monsoon generates anomalous northeasterly winds in the northeastern Indian Ocean. The easterly component of these anomalous winds produces upwelling and surface cooling in the equatorial eastern Indian Ocean throughout the year.

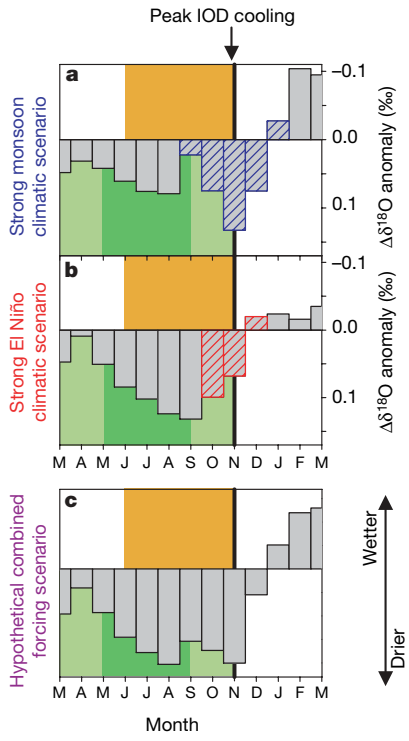

Figure 4 | Composite records of IOD drought. Composite IOD drought signals during a single monsoon cycle for the strong monsoon (**a**) and strong El Niño climatic scenarios (**b**). Bars with coloured hatching show $\Delta\delta^{18}O$ values that correspond to strong (exceeding 1.6 °C) cool SST anomalies. Vertical line denotes peak IOD cooling. Approximate periods of the transition and summer phases of the Asian monsoon are denoted by light and dark green shading, respectively. Orange shading shows the present-day timing of El Niño-driven droughts in western Indonesia. **c**, Also shown is a hypothetical 'combined IOD drought' scenario where IOD conditions are forced synergistically both by strong El Niño and by strong monsoon conditions, such as could occur with projected ENSO-independent strengthening of the Asian monsoon.

The simulation results indicate that the prolonged cooling during mid-Holocene IOD events may reflect an earlier development of anomalous Ekman upwelling in the eastern IOD sector, due to stronger cross-equatorial winds driven by enhanced summer warming of the Asian landmass in the middle Holocene[17,25]. Another possibility, suggested by the simulations of mid-Holocene monsoon dynamics, is that prolonged cooling during IOD events could result from stronger summer monsoon winds superimposed on a strengthened equatorial easterly wind field. The prolonged IOD cooling during the strong monsoon scenario is also consistent with model studies of IOD initiation processes, which suggest that IOD events triggered by processes internal to the Indian Ocean tend to begin earlier than those triggered by El Niño events in the Pacific[7,8].

The composite IOD reconstructions show that drought is a key feature associated with IOD events in both the strong monsoon and strong El Niño climatic scenarios (Fig. 3). In both scenarios the $\Delta\delta^{18}O$ anomalies suggest that rainfall is reduced for almost the entire year leading up to peak IOD conditions. However, the nature and timing of peak drought conditions are quite different for the two climatic scenarios (Fig. 4). During the strong El Niño setting of the late Holocene, the $\Delta\delta^{18}O$ record indicates that eastern IOD droughts have a single main dry phase that is synchronous with the timing of El Niño-driven droughts in western Indonesia (~June–November)[26]. Moreover, the drought peaks before strong (greater than 1.6 °C) IOD cooling occurs (Fig. 4b). Hence, it appears that the relatively brief period of strong IOD cooling in this climatic scenario restricts eastern IOD droughts primarily to the duration of drying expected from El Niño conditions alone. The composite IOD reconstruction for the strong El Niño climatic scenario also shows a period of drought in the second year after peak IOD conditions (Fig. 3). This is a robust feature of each of the individual IOD events from the late Holocene (Supplementary Fig. 3), and may be related to the biennial nature of the IOD noted in some studies[1,2].

In contrast, droughts in the eastern IOD region during the middle Holocene tended to be bimodal and peaked later (Fig. 4a). In this strong monsoon scenario, the early phase of IOD drought corresponds with the Asian summer monsoon season (~May–September) and is probably caused by strengthened cross-equatorial airflow drawing moisture from the tropical Indian Ocean into the Asian monsoon. A second, and more prominent, dry phase develops later and is synchronous with the extended period of strong (greater than 1.6 °C) IOD cooling in this climatic scenario. This suggests that prolonged cooling in the tropical eastern Indian Ocean can also play a direct role in driving IOD droughts in western Indonesia.

These findings are supported by our simulations of mid-Holocene sea surface salinity (Fig. 2c), which show a region of increased salinity extending from the coast of Sumatra into the Bay of Bengal. This salinity anomaly is associated with enhanced surface-ocean evaporation driven by strengthened Asian monsoon winds. The simulated cooling of SSTs in the tropical eastern Indian Ocean (Fig. 2b) also drives anomalous atmospheric subsidence and divergence, which reduces precipitation. These eastern IOD drought processes during the middle Holocene are also consistent with the simulated droughts produced in models of El Niño-independent IOD events[8].

The coral records and model simulations demonstrate that both ENSO and the Asian monsoon are capable of influencing drought

dynamics in the eastern IOD sector. Historically these influences on the IOD have tended to oppose each other, because El Niño conditions have generally led to weaker monsoons. However, there is evidence indicating that this tight coupling of the Asian monsoon and ENSO systems has begun to break down over recent decades[6]. The weakening of this relationship may be due to systematic changes in the pattern of Pacific SST anomalies during El Niño events[27], or due to transient greenhouse warming of the Eurasian landmass which has enabled ENSO-independent strengthening of the Asian monsoon[6,21,22]. During the twenty-first century it is expected that greenhouse warming will cause the Asian monsoon to strengthen further[21,22]; however, light-scattering aerosols and land-clearing may initially reduce monsoon strength before aerosol-control policies and greenhouse-gas emissions lead to an abrupt return of a more intense Asian monsoon[23].

Our findings raise the possibility that the extent of the rural challenges posed by future changes in Asian monsoon strength may have been underestimated. In particular, the later peak that we observe in IOD droughts during the strong monsoon scenario of the middle Holocene coincides with the time when rainfall in western Indonesia is normally at its annual maximum (Supplementary Fig. 4). Hence, the consequences of such a change in the timing of maximum IOD drought conditions may be particularly severe. Recent changes in the ENSO–monsoon relationship further raise the possibility that IOD droughts could intensify in the future if monsoon forcing acts synergistically with El Niño (Fig. 4c). Hence, while predictions of changing monsoon strength have focused on impacts in Asia and India[23,28], any ENSO-independent strengthening of the Asian monsoon will probably serve to prolong IOD-related droughts in western Indonesia, and possibly also southern Australia[3], thus adding to the socio-economic impacts of the IOD.

Received 10 May; accepted 21 November 2006.

1. Webster, P. J., Moore, M. D., Loschnigg, J. P. & Leben, R. R. Coupled ocean–atmosphere dynamics in the Indian Ocean during 1997–98. *Nature* **401,** 356–360 (1999).
2. Saji, H. H., Goswami, B. N., Vinayachandran, P. H. & Yamagata, T. A dipole mode in the tropical Indian Ocean. *Nature* **401,** 360–363 (1999).
3. Ashok, K., Guan, Z. & Yamagata, T. Influence of the Indian Ocean Dipole on the Australian winter rainfall. *Geophys. Res. Lett.* **30,** 1821, doi:10.1029/2003GL017926 (2003).
4. Abram, N. J., Gagan, M. K., McCulloch, M. T., Chappell, J. & Hantoro, W. S. Coral reef death during the 1997 Indian Ocean Dipole linked to Indonesian wildfires. *Science* **301,** 952–955 (2003).
5. Birkett, C., Murtugudde, R. & Allan, T. Indian Ocean climate event brings floods to East Africa's lakes and the Sudd Marsh. *Geophys. Res. Lett.* **26,** 1031–1034 (1999).
6. Kumar, K. K., Rajagopalan, B. & Cane, M. A. On the weakening relationship between the Indian Monsoon and ENSO. *Science* **284,** 2156–2159 (1999).
7. Behera, S. K. *et al.* A CGCM study on the interactions between IOD and ENSO. *J. Clim.* **19,** 1688–1705 (2006).
8. Fischer, A. S., Terray, P., Guilyardi, E., Gualdi, S. & Delecluse, P. Two independent triggers for the Indian Ocean Dipole/Zonal Mode in a coupled GCM. *J. Clim.* **18,** 3428–3449 (2005).
9. Charles, C. D., Cobb, K. M., Moore, M. D. & Fairbanks, R. G. Monsoon-tropical ocean interaction in a network of coral records spanning the 20th century. *Mar. Geol.* **201,** 207–222 (2003).
10. Beck, J. W. *et al.* Sea-surface temperatures from coral skeletal strontium/calcium ratios. *Science* **257,** 644–647 (1992).
11. Gagan, M. K. *et al.* Temperature and surface-ocean water balance of the mid-Holocene tropical western Pacific. *Science* **279,** 1014–1018 (1998).
12. Briggs, R. W. *et al.* Deformation and slip along the Sunda Megathrust in the great 2005 Nias-Simeulue earthquake. *Science* **311,** 1897–1901 (2006).
13. Reynolds, R. W. & Smith, T. M. Improved global sea surface temperature analyses using optimum interpolation. *J. Clim.* **7,** 929–948 (1994).
14. Charles, C. D., Hunter, D. E. & Fairbanks, R. G. Interaction between the ENSO and the Asian monsoon in a coral record of tropical climate. *Science* **277,** 925–928 (1997).
15. Eaton, P. & Radojevic, M. *Forest Fires and Regional Haze in Southeast Asia* (Nova Science Publishers, Huntington, New York, 2001).
16. Sontakke, N. A., Pant, G. B. & Singh, N. Construction of all-India summer monsoon rainfall series for the period 1844–1991. *J. Clim.* **6,** 1807–1811 (1993).
17. Yuan, D. *et al.* Timing, duration, and transitions of the Last Interglacial Asian monsoon. *Science* **304,** 575–578 (2004).
18. Moy, C. M., Seltzer, G. O., Rodbell, D. T. & Anderson, D. M. Variability of El Nino/Southern Oscillation activity at millennial timescales during the Holocene epoch. *Nature* **420,** 162–165 (2002).
19. Gagan, M. K., Hendy, E. J., Haberle, S. G. & Hantoro, W. S. Post-glacial evolution of the Indo-Pacific Warm Pool and El Nino-Southern Oscillation. *Quat. Int.* **118–119,** 127–143 (2004).
20. Koutavas, A., Lynch-Stieglitz, J., Marchitto, T. M. & Sachs, J. P. El Nino-like pattern in Ice Age tropical Pacific sea surface temperature. *Science* **297,** 226–230 (2002).
21. Ashrit, R. G., Kumar, K. R. & Kumar, K. K. ENSO-monsoon relationships in a greenhouse warming scenario. *Geophys. Res. Lett.* **28,** 1727–1730 (2001).
22. Hu, Z.-Z., Latif, M., Roeckner, E. & Bengtsson, L. Intensified Asian summer monsoon and its variability in a coupled model forced by increasing greenhouse gas concentrations. *Geophys. Res. Lett.* **27,** 2681–2684 (2000).
23. Zickfeld, K., Knopf, B., Petoukhov, V. & Schellnhuber, H. J. Is the Indian summer monsoon stable against global change? *Geophys. Res. Lett.* **32,** L15707, doi:10.1029/2005GL022771 (2005).
24. Liu, Z., Brady, E. & Lynch-Stieglitz, J. Global ocean response to orbital forcing in the Holocene. *Paleoceanography* **18,** 1041, doi:10.1029/2002PA000819 (2003).
25. Liu, Z., Harrison, S. P., Kutzbach, J. & Otto-Bliesner, B. Global monsoons in the mid-Holocene and oceanic feedback. *Clim. Dyn.* **22,** 157–182 (2004).
26. Dai, A. & Wigley, T. M. L. Global patterns of ENSO-induced precipitation. *Geophys. Res. Lett.* **27,** 1283–1286 (2000).
27. Kumar, K. K., Rajagopalan, B., Hoerling, M., Bates, G. & Cane, M. Unraveling the mystery of Indian monsoon failure during El Nino events. *Science* **314,** 115–119 (2006).
28. Anderson, D. M., Overpeck, J. T. & Gupta, A. K. Increase in the Asian southwest monsoon during the past four centuries. *Science* **297,** 596–599 (2002).
29. Xie, P. & Arkin, P. A. Analyses of global monthly precipitation using gauge observations, satellite estimates, and numerical model predictions. *J. Clim.* **9,** 840–858 (1996).

Supplementary Information is linked to the online version of the paper at www.nature.com/nature.

Acknowledgements We thank D. Prayudi, I. Suprianto, K. Glenn, T. Watanabe, H. Scott-Gagan, K. Sieh and the Indonesian Institute of Sciences (LIPI) for assistance with fieldwork, which was carried out under research permits issued by LIPI. We thank H. Scott-Gagan, J. Cali, G. Mortimer, A. Alimanovic and D. Kelleher for laboratory assistance, and R. Gallimore and P. Behling for the model simulations and model output processing. This study was supported by an Australian Postgraduate Award and RSES Jaeger Scholarship to N.J.A., and an Australian Research Council Discovery grant to M.K.G. and W.S.H.

Author Contributions N.J.A. was responsible for coral geochemical analysis and interpretation of the records. M.K.G. was Chief Investigator and the Australian Institutional Counterpart for the ARC project. Z.L. provided climate model simulations and advice on ocean–atmosphere interactions. W.S.H. was Partner Investigator and the Indonesian Institutional Counterpart for the ARC project. M.T.M. supported the TIMS Sr/Ca analyses. B.W.S. provided extensive logistical support for fieldwork. N.J.A and M.K.G. wrote the paper, with comments provided by all other authors.

Author Information Reprints and permissions information is available at www.nature.com/reprints. The authors declare no competing financial interests. Correspondence and requests for materials should be addressed to N.J.A. (nabr@bas.ac.uk) and M.K.G. (michael.gagan@anu.edu.au).